

## COMPARATIVE STUDY OF ADDITIVELY MANUFACTURED INCONEL 625 IN THE AS-BUILT AND HEAT-TREATED CONDITION

V. Luna<sup>a, b</sup>, L. Trujillo<sup>a, c</sup>, A. Gamon<sup>a, c</sup>, L. Marquez<sup>a, b</sup>, E. Arrieta<sup>a, b</sup>, L. E. Murr<sup>a, c</sup>, R. B.  
Wicker<sup>a, b</sup>, C. Katsarelis<sup>d</sup>, P. R. Gradl<sup>d</sup>, and F. Medina<sup>a, b</sup>

<sup>a</sup> W.M. Keck Center for 3D Innovation, The University of Texas at El Paso, El Paso, TX 79968, USA

<sup>b</sup> Department of Aerospace and Mechanical Engineering, The University of Texas at El Paso, TX 79968, USA

<sup>c</sup> Department of Metallurgical, Materials and Biomedical Engineering, The University of Texas at El Paso, TX  
79968, USA

<sup>d</sup> NASA, Marshall Space Flight Center, Huntsville, AL 35812, USA

### Abstract

This study was conducted to characterize the microstructure and mechanical properties of Inconel 625 manufactured with laser powder bed fusion (L-PBF), electron beam melting (EBM), wire arc additive manufacturing (WAAM), electron beam directed energy deposition (EB-DED), laser powder directed energy deposition (LP-DED), and laser wire directed energy deposition (LW-DED) in both the as built and heat-treated condition. The heat treatment in this study included stress relieving, hot isostatic pressure (HIP), and solution treatment. The effects of the heat treatment on the grain widths and hardness of the alloy will be observed across the technologies before and after heat-treatment. At the end of this study there will be a comparative analysis of the alloy Inconel 625 across the six technologies.

**Keywords:** Inconel 625, Additive manufacturing techniques, Post-process heat treatment, Microstructures, Microindentation hardness, Tensile properties.

### Introduction

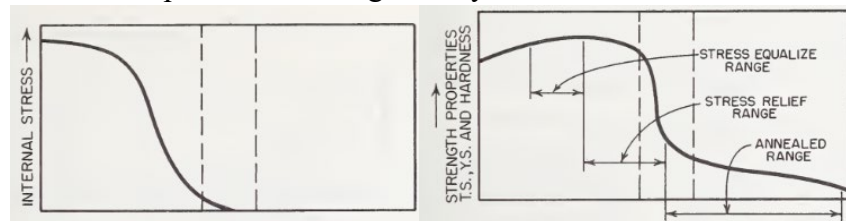
Before the advent of additive manufacturing (AM), the design process for applications of nickel-base super alloys such as Inconel 625 consisted primarily of schedules of heat treatments of wrought and cast products which allowed for the manipulation of precipitates, especially gamma double prime, and the subsequent control of residual mechanical properties [1-3]. With the establishment of AM processing, not only were the as-built components different from wrought or cast components on comparing residual microstructures and mechanical properties, but also the resulting heat treatments of these AM components as well [4-7]. In addition, various types of AM processing also produced specific, as-built component microstructures and associated mechanical properties depending upon process parameters utilized [8,9], and these associated microstructures

and mechanical properties could also be variously manipulated by subsequent heat treatments as well [5-7].

Metal additive manufacturing has become a valued asset to the manufacturing of aerospace applications because of the opportunities it provides [7]. These opportunities include: unique design solutions, ability to use otherwise difficult to manufacture materials like novel alloys, considerable reduction in lead time and cost, and mass reduction through efficient and lightweight designs able to be created. Many metal AM processes have been created and studied, each having their advantages and disadvantages for fabricating parts. A critical aspect of product design is the ability to exchange and select AM processes to fit design and manufacturing constraints such as process cost, part complexity, build volume, post-build operations like heat-treatment, and desired material characteristics including microstructure and mechanical properties [8].

Heat treatment of alloys can in general relieve internal stresses, reduce porosity by hot isostatic pressing (HIP), and provide precipitation strengthening or hardening through aging. In addition, high temperature heat treatment above about 1100 °C for super alloys like Inconel 625 will initiate recrystallization and grain growth. Figure 1 provides a general overview of the heat treatment processes.

Gamon et al. [8] recently provided a breakdown and comparison of nine different AM processes that compare microstructure and micro hardness of as-built specimens of Inconel 625 alloy from each process. The present study builds upon Gamon et al.'s approach [8] of comparing Inconel 625 alloy across different AM technologies with the added post-process heat-treatment. This addresses a challenge in the aerospace industry of certifying parts, where the AM process needs to be thoroughly understood and the components manufactured to fulfill repeatable design, quality and safety requirements and standards can be fulfilled [7]. Studying the microstructure and mechanical properties for post heat-treatment of these specimens is a crucial part of continuing this study because most components are not generally utilized in their as-built condition [7,9]. In



addition, while numerous studies have examined and compared post-process heat treatments with specific as-built AM process products [5-7,9], the present study compares a range of AM process as-built and post process heat treated components; thereby expanding the design and application optimization window as it applies to Inconel 625 alloy applications [7].

**Figure 1.** Effect of Temperature on Metal Alloys Heat Treatment (After ref. 10).

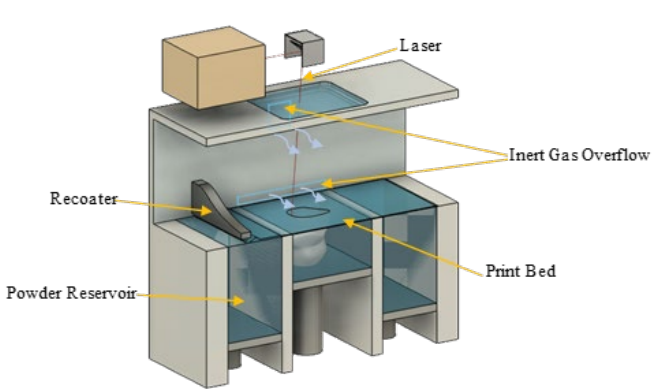
## **Materials and Methods**

### *Additive Manufacturing Processes and Processing Parameters*

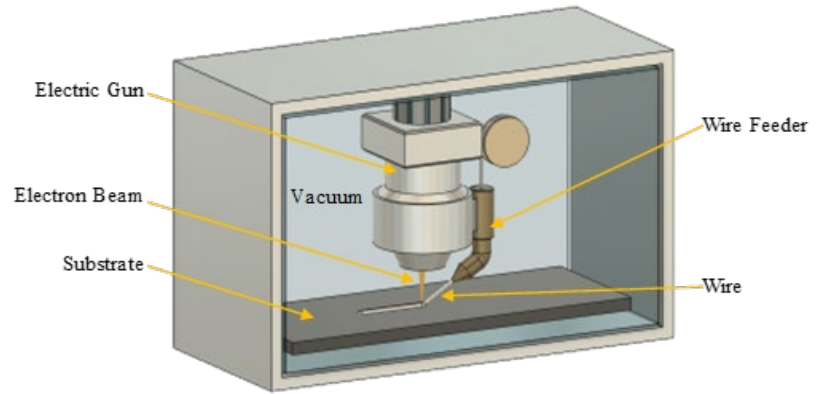
This study involves 6 different additive manufacturing techniques or processes utilizing wire or powder fusion. These include: Laser powder-bed fusion (L-PBF), Electron beam directed energy deposition (EB-DED), Wire-arc additive manufacturing (WAAM), Electron beam powder bed fusion (EB-PBF), Laser powder directed energy deposition (LP-DED), and Laser wire directed energy deposition (LW-DED). These processes are

illustrated generally in Figure 2. It is observed that three processes involve wire feed while three processes involve powder feed or a powder bed. All but the WAAM processes utilize electron or laser beam melting. Gamon, et al. [8] have briefly discussed these process techniques in more detail.

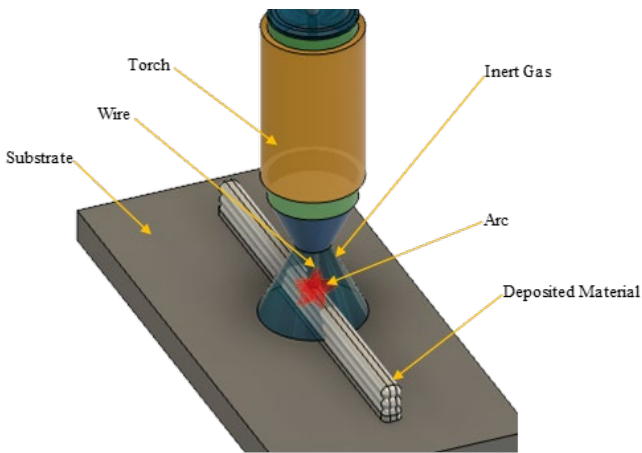
Multiple specimens representing the six AM processes investigated in this study were received and include L-PBF, WAAM, EB-DED, LP-DED, EB-PBF, and LW-DED. The parameters used to build each sample are provided in Table 1. In Table 2 an index of each sample is provided along with a description of the geometries of the as-built specimens. For the LP-DED and LW-DED different specimens were created to observe any change in microstructure or mechanical property between the varying parameters. The LP-DED had the same build specifications except for the power of the laser, five laser powers ranging from 350W to 2620W are included in this study. The LW-DED samples have a variation only in the tool path used in the build. For example, the raster 90 tool path is angled 90° from the x-axis of the build table, Figure 3 shows this tool path. Raster is a 0° raster tool path and the linear sample follows a path around the perimeter with a 45° infill.



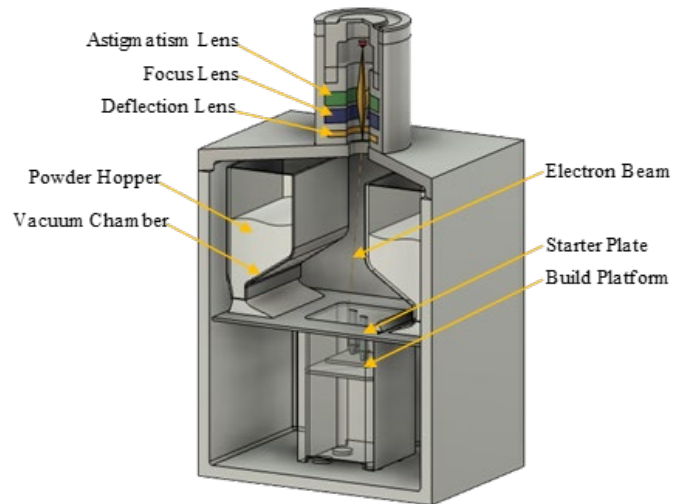
Laser Powder Bed Fusion



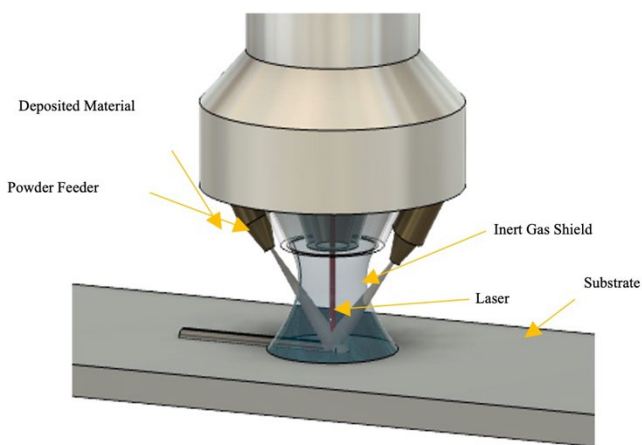
Electron Beam Directed Energy Deposition



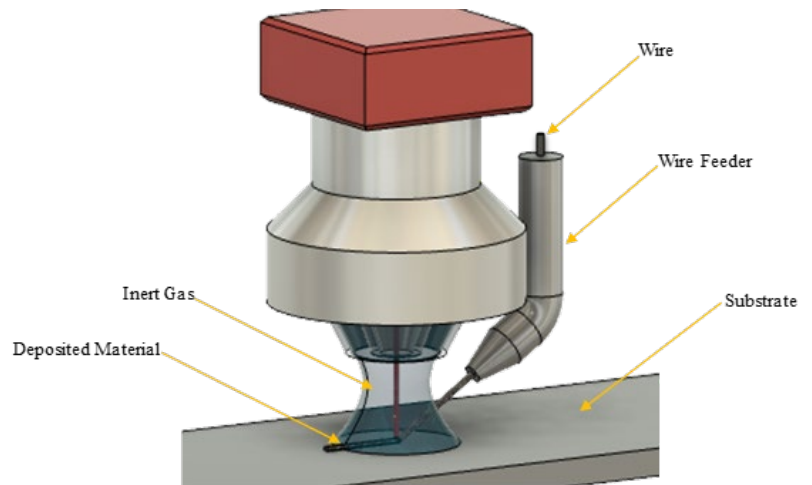
Wire Arc Additive Manufacturing



Electron Beam Powder Bed Fusion



Laser Powder Directed Energy Deposition



Laser Wire Directed Energy Deposition

**Figure 2.** AM process schematic visualizations for layer-building techniques used in this research.

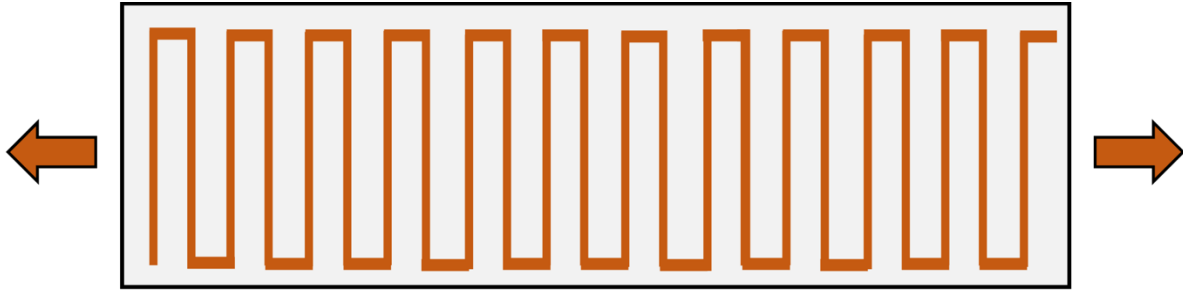


**Figure 3.** LW-DED Raster 90 toolpath

**Table 1.** As-built AM process parameters

Sample	Machine	Type Feedstock	Size	Power (W)	Travel Speed (mm/s)	Layer Thickness (µm)
L-PBF	EOS M400-4	Powder	15 - 45 µm	180	1000	40
WAAM	Lincoln Electric Pulsed MIG / Fanuc Robot	Wire	1.57 mm dia	-	-	-
EB-DED	Sciaky	Wire	1.57 mm dia	4800	12.7	-
LP-DED - 350W	RPM Innovations 557	Powder	45 - 150 µm	350	16.9	-
LP-DED - 700W	RPM Innovations 557	Powder	45 - 150 µm	750	16.9	-
LP-DED - 1070W	RPM Innovations 557	Powder	45 - 150 µm	1070	16.9	-
LP-DED - 2000W	RPM Innovations 557	Powder	45 - 150 µm	2000	16.9	-
LP-DED - 2620W	RPM Innovations 557	Powder	45 - 150 µm	2620	12.7	-
EB-PBF	Arcam	Powder	45 - 106 µm	900	1080	50
LW-DED Raster	Meltio M450	Wire	1.12 mm dia	870	9.8	-
LW-DED Raster 90	Meltio M450	Wire	1.12 mm dia	870	9.8	-
LW-DED Linear 1	Meltio M450	Wire	1.12 mm dia	870	10.0	-

**Table 2.** AM as-built sample identification and geometries

Specimen Index			
Additive Manufacturing Process	Sample ID	As Received Geometry	Etchant Time (s)
L-PBF	B.1	Z-Oriented Cylinder	60±10
WAAM	C.1	Z- Oriented Flat Bar	90±10
EB-DED	D.1	Z- Oriented Flat Bar	90±10
LP-DED 350W	G.1	Z- Oriented Flat Bar	90±10
LP-DED 700W	G.2	Z- Oriented Flat Bar	90±10
LP-DED 1070W	G.3	Z- Oriented Flat Bar	90±10
LP-DED 2000W	G.4	Z- Oriented Flat Bar	90±10
LP-DED 2620W	G.5	Z- Oriented Flat Bar	90±10

<b>EB-PBF</b>	H.1	Square Prism	90±10
<b>LW-DED Raster</b>	I.1	Z-Oriented Flat Bar	90±10
<b>LW-DED Raster 90</b>	I.2	Z-Oriented Flat Bar	90±10
<b>LW-DED Linear</b>	I.3	Z-Oriented Flat Bar	90±10

Table 1 compares the primary build parameters for the AM processes utilized in this study (Figure 2). Only the WAAM process utilizes arc melt parameters which are not readily measurable. Generally, laser and electron beam melting involve beam power, P, or power density, Q, in Watts, where  $Q \sim P/v$ ; and v is the beam travel or scan speed in mm/s (Table 1). For most metals and alloys involved in laser or electron beam processes (Figure 2), the as-built microstructure depends on the so-called temperature gradient, G, and the growth rate, R, where the layer cooling rate is correspondingly expressed as  $G.R \sim e^{aQ}$ ; and a is a constant.[9]. It is also generally observed that increasing cooling rates (G.R) promote a decreasing microstructure size. Additionally, decreasing G/R promotes columnar-to-equiaxed grain structures in the as-built products [9]. Table 1 illustrates that a range of processing power ranging from 350 to 2620 Watts was selected for the LP-DED AM processing. While Table 1 shows the powder size/size distribution and wire diameter for specific AM machines utilized in this study, Table 2 shows the residual specimen or component geometries with identification coding (sample ID), along with etching times for metallographic specimen preparation.

For this study, all of the samples represented in Tables 1 and 2 were heat treated. The heat treatment involved stress relieving (SR) at 1066 °C for 1.5 hours, HIP at 1163 °C for 3 or 4 hours in inert gas at 15 ksi pressure (ASTM 3301-18a standard), followed by solution treatment (SOL) at 1177 °C for 1 hour; with furnace cooling per AMS 7000/AMS 2774 standard: (SR + HIP + SOL).

### *Metallographic Preparation*

The build direction microstructure was revealed by sectioning as-built samples with an ATM Brilliant 220 precision cutter. To avoid incorrect interpretation of micrographs and material characteristics, samples having a substrate of different material were sectioned and studied at an apparent distance away from the fusion zone. Metallographic samples of the sectioned specimens were created using a combination of powdered epoxy and phenolic acid and a hot mounting press from ATM OPAL (Haan, Germany). Grinding and polishing were done after the samples were mounted to produce a mirror-like surface.

The grinding and polishing procedures were conducted with an ATM SAPHIR 530 semi-automatic system. The grinding procedure started with a 240-grit coarse Si-C (Silicon carbide) grinding paper, followed by grits 320, 400, 600, and 800 each was spun at 300 RPM with a force of 25N for 1 minute using water as a lubricant. The polishing procedure was carried out at a speed of 150 RPM and a force of 25 N for 5 minutes, with each stage of the polishing process having a different nylon disk for the 6 m, 3 m, and 1 m diamond slurries. Finally, the samples were polished for 2 minutes at 150 RPM with a force of 35 N using a short synthetic nap disk and a 0.5 m AlO<sub>2</sub> (Alumina) slurry. The samples were ultrasonicated prior to polishing and in between each polishing stage to eliminate cross-contamination.

The etchant was a variation of ASTM E407 etchant 149. The solution consisted of 25 ml of hydrochloric acid, 15 ml lactic acid, and 3 ml of hydrogen peroxide. Submersion of the specimens in the etching solution for a range of 45 to 90 seconds was the etching procedure in this investigation. The optical micrographs in this work were taken with an Olympus GX53 inverted optical microscope (Olympus Inc., Tokyo, Japan).

### *Hardness Testing*

Micro-indentation hardness was completed at NASA Marshall Space Flight Center with a Struers Durascan indenter. Indentations were made with a Vickers indenter and a load of 300 gf, and measured with a 50X objective lens. At least ten measurements were taken for each sample variation.

### *Grain Width/Size Measurements*

The line intercept technique, as published in ASTM E112, was used to compute grain width measurement. The freeware ImageJ was used to draw and measure straight lines across the micrograph. The number of grain boundaries intercepted was counted until at least 100 grain boundaries were intercepted [10]. Since etching only showed the dendrite ends, these measurements were frequently supplemented by hand measurements of interdendritic spacings.

### *Tensile Tests*

Tensile testing of the specimens was conducted at Westmoreland Mechanical Testing & Research, Inc. according to ASTM E8-21. Tensile tests also included the examination of selected fracture surfaces using scanning electron microscopy (JEOL JMS-IT500 SEM).

## **Results and Discussion**

### *Microstructures and Microstructure Comparisons*

Figure 12 shows a very notable difference between the as-built AM process microhardness and those observed for post-process heat treatment. The micro indentation hardness for the as-built columnar structure in Sample H. 1 averaged HV 191 in contrast to the as-built L-PBF where the hardness averaged HV 305, and the LW-DED sample I. 3 where the hardness averaged HV 220.

The corresponding micro indentation hardness for the heat treated EB-DED AM process component was HV 186 while in contrast it was HV 206 for the heat treated L-PBF and only HV 180 for the heat treated WAAM. This micro indentation hardness difference between the heat-treated L-PBF and WAAM microstructures is consistent with the grain size difference: decreasing grain size and correspondingly increasing hardness. This feature was also observed for the LP-DED process series where the 350 W power component after heat treatment had a grain width/size of 62 microns and a hardness of HV 191 in contrast to the 2620 W power component with a grain size of 114 microns and

a hardness of HV 187. An exception to this trend is the AM processed EB-PBF component where the as-built columnar grain width is 15 microns in contrast to the heat-treated component columnar grain width of ~ 150 microns; each having the same micro indentation hardness of HV 191. The trend of increasing hardness with decreasing grain size is, however followed for the LW-DED AM process series where the heat-treated raster grain size of 109 microns and a hardness of HV 209 is in contrast to the linear 1 grain size of HV 72 and a corresponding hardness of HV 220.

*Microstructure and Mechanical Property Comparisons and Discussion*

Tables 3 and 4 list and summarize the as-built and heat-treated Inconel 625 AM process component properties; including residual densities, grain morphologies and nominal grain widths, Vickers micro indentation hardness (HV), and tensile properties (yield stress, UTS, and elongation (%)) in the case of the heat-treated components in Table 4. Complimenting these tables, Figures 5 and 6 show comparative bar graphs for the average grain widths and micro hardness measurements, respectively, for as-built and heat-treated AM process components utilizing the data in Tables 3 and 4.

<b>AM Process</b>	<b>Achieved Density (%)*</b>	<b>Grain Morphology</b>	<b>Grain Width (µm)</b>	<b>Hardness (HV)</b>
L-PBF (B.1)	99.8	Columnar/Dendrites	75 ±7	304 ±7
WAAM (C.1)	99.9	Columnar/Dendrites	129 ±18	228 ±4
EB-DED (D.1)	99.9	Columnar/Dendrites	54±5	236 ±6
LP-DED 350W (G.1)	99.9	Columnar/Dendrites	43±5	263 ±7
LP-DED 750W (G.2)	99.9	Columnar/Dendrites	90±8	256 ±9
LP-DED1070W (G.3)	99.8	Columnar/Dendrites	71±6	242 ±6
LP-DED 2000W (G.4)	99.9	Columnar/Dendrites	92±7	242 ±7
LP-DED 2620W (G.5)	99.5	Columnar/Dendrites	117±14	223 ±9
EB-PBF (H.1)	99.1	Columnar	15±23	191 ±6
LW-DED Raster (I.1)	99.9	Columnar/Dendrites	80 ±8	223 ±9

**Table 3.** Summary of AM Process Microstructures and Related Properties of As-built Components

\* The density measurements were made using gas displacement pycnometry for volume measurements and a Sartorius balance system for weight.

**Table 4.** Summary of AM Process Microstructures, Mechanical and Related Properties for heat treated (SR + HIP + SOL) components.

<b>AM Process</b>	<b>Achieved Density (%)</b>	<b>Grain Morphology</b>	<b>Grain Width (<math>\mu\text{m}</math>)</b>	<b>Hardness (HV)</b>	<b>UTS (MPa)</b>	<b>Yield Strength (MPa)</b>	<b>% Elongation</b>
L-PBF (B.1)	99.9	Equiaxed	45 $\pm$ 7	206 $\pm$ 11	855	371	55.7
WAAM (C.1)	99.9	Equiaxed	330 $\pm$ 4	180 $\pm$ 8	659	285	56
EB-DED (D.1)	99.9	Equiaxed	168 $\pm$ 6	186 $\pm$ 9	742	305	70.2
LP-DED 350W (G.1)	99.9	Equiaxed	62 $\pm$ 7	191 $\pm$ 10	849	354	61
LP-DED 750W (G.2)	99.9	Equiaxed	92 $\pm$ 9	188 $\pm$ 11	812	335	64
LP-DED1070W (G.3)	99.9	Equiaxed	77 $\pm$ 6	188 $\pm$ 10	817	334	62.9
LP-DED 2000W (G.4)	99.9	Equiaxed	94 $\pm$ 7	191 $\pm$ 13	792	334	61.8
LP-DED 2620W (G.5)	98.9	Equiaxed	114 $\pm$ 9	187 $\pm$ 9	740	336	60.5
EB-PBF (H.1)	99.9	Columnar	150 $\pm$ 6	188 $\pm$ 9	731	321	55.6
LW-DED Raster (I.1)	99.9	Equiaxed	109 $\pm$ 8	209 $\pm$ 14	754	305	54.8
LW-DED Raster 90 (I.2)	99.9	Equiaxed	103 $\pm$ 10	215 $\pm$ 26	754	313	51.6
LW-DED Linear 1(I.3)	99.5	Equiaxed	72 $\pm$ 4	220 $\pm$ 22	768	326	52.2

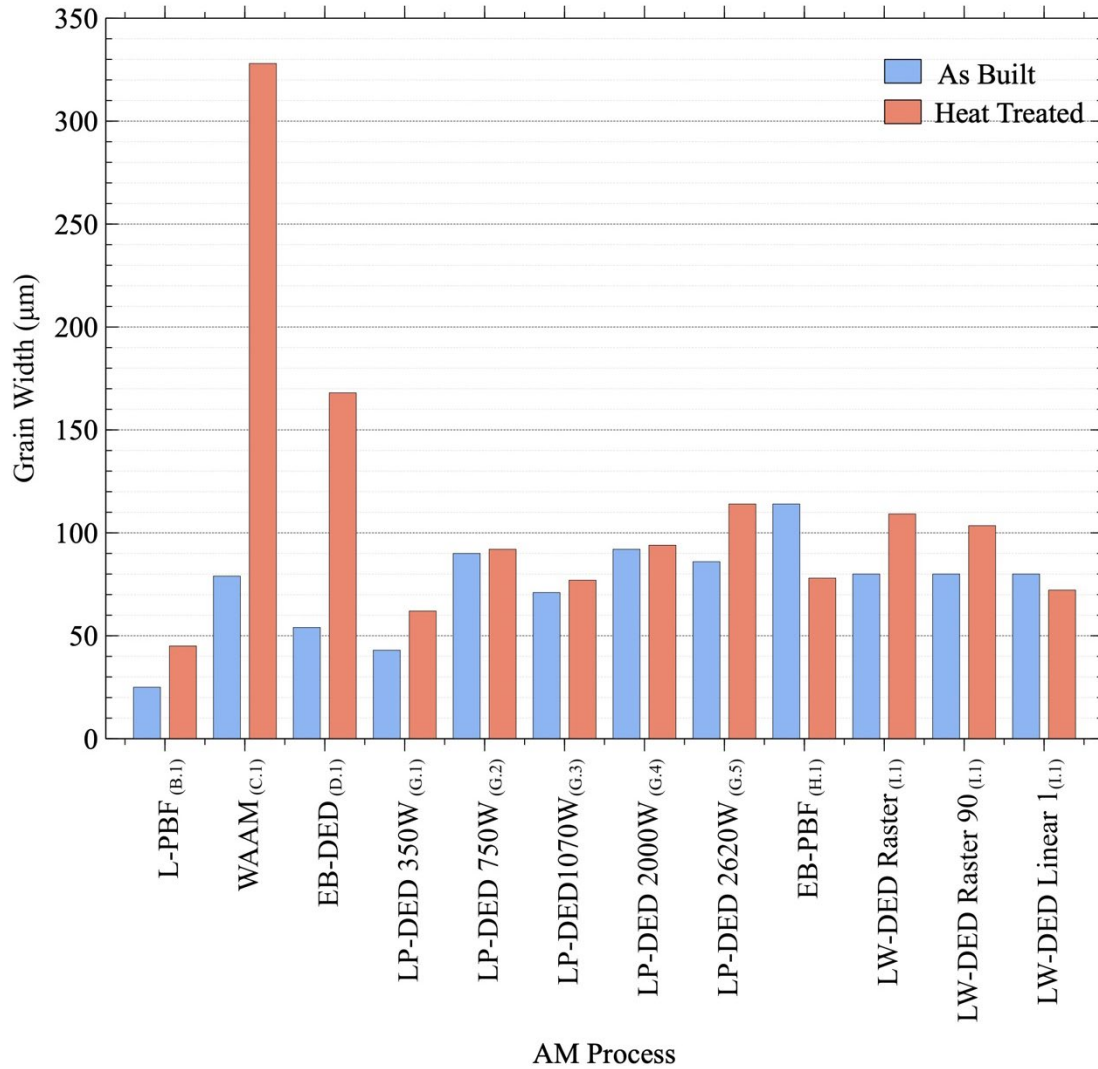


**Figure 5.** Direct comparison of AM process grain widths for as-built and heat-treated components

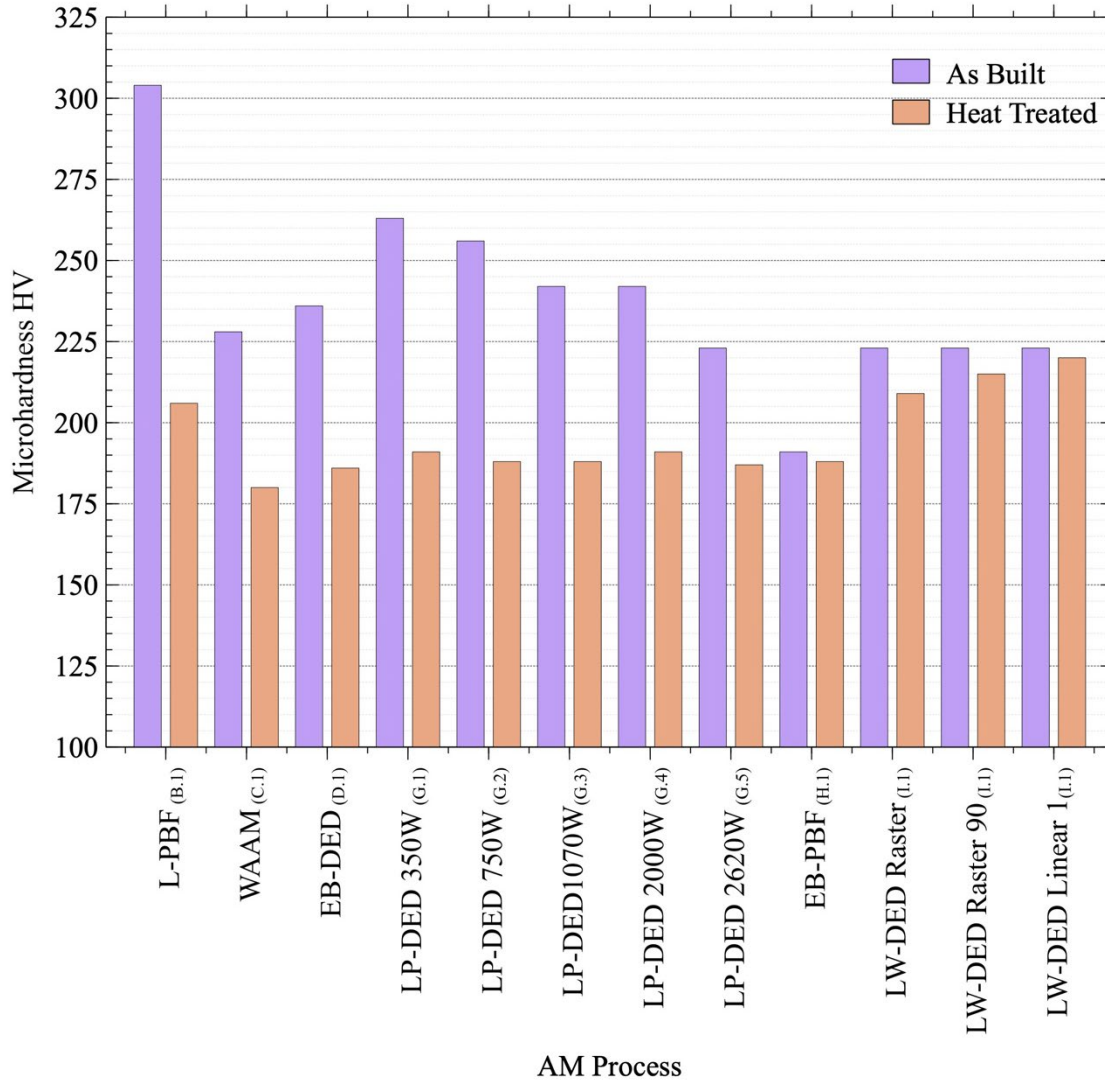


**Figure 6.** Comparison of micro hardness in the as-built versus heat treated condition for AM processes.

A notable feature in Figures 5 and 6 is the generally increasing hardness with decreasing grain width. Figure 7 shows little change of the yield stress and UTS over the range of heat-treated AM process components with the exception of the WAAM and EB-DED products which exhibit the largest grain widths. The EB-DED heat treated component also shows the largest elongation of 70.2 % (Table 4). While the heat treatment of the various AM processes varied from HV 191 to HV 220 (Table 4) - a variance of 15 %, the as-built variance was HV 191 to HV 304, or 59 %. The corresponding as built yield strength varied from 285 MPa for the heat treated WAAM sample to 371 MPa for the L-PBF sample, a variance of 30 % (Table 4). The corresponding elongations for the heat-treated AM process components varied from a low of ~ 52 % to a high of ~ 70 % as noted above; a variance of 35 % (Table 4). These results indicate a relatively wide window for mechanical property manipulation for the heat treatment of a variety of AM processes as presented in Figure 2.

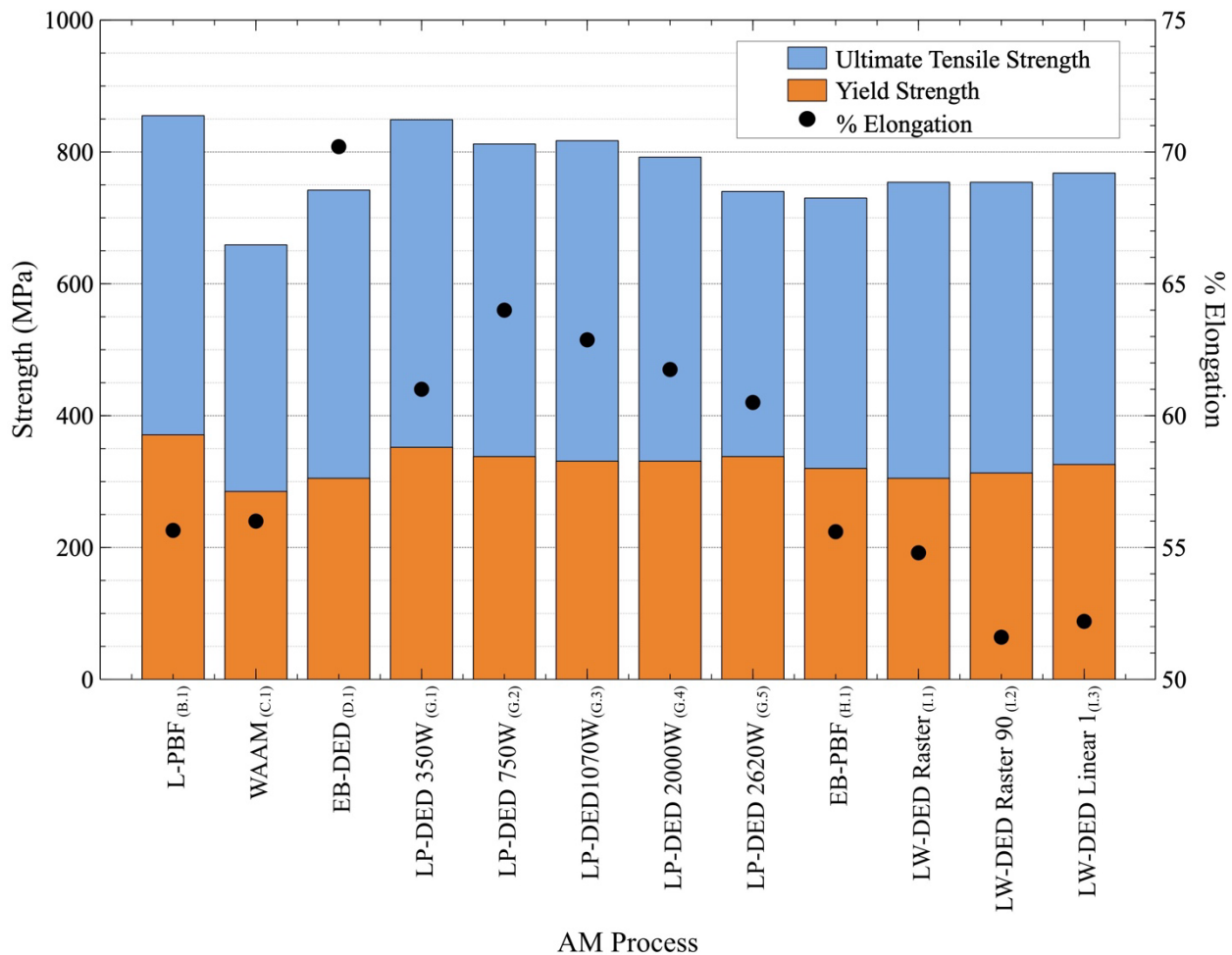


**Figure 7.** Summary of the ultimate tensile and yield strength of the specimens for heat treated AM process components.

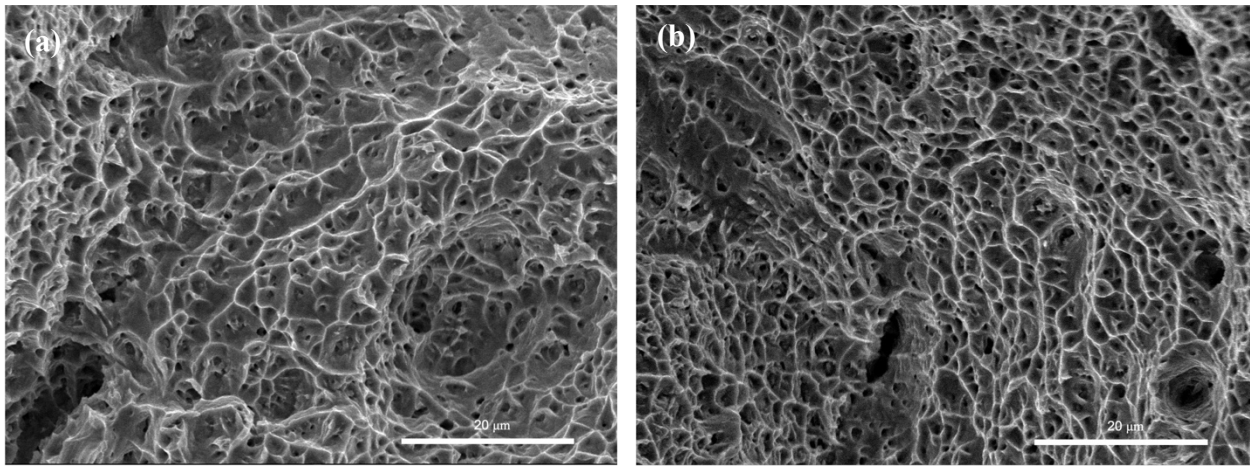
As noted above, the high temperatures associated with the current heat treatment of variously produced AM process components dominated the residual microstructure production, forming recrystallized grains containing annealing twins and carbide precipitates, neither of which seems to have a significant effect on the residual mechanical properties. Recrystallization and resulting grain growth has the advantage of eliminating anisotropy in laser bed fusion produced Inconel 625 alloy [15]. Lower temperature heat treatment below the solubility temperature for gamma double prime precipitates (<700 ° C) [1-3] may allow additional mechanical property manipulation for these AM processes (Figure 2).

### *Fracture Surface Observations and Discussion*

SEM images showing fracture surface features for the heat treated, AM processed components generally exhibited ductile dimples having dimple sizes ranging from 2-5 microns. The largest dimple sizes of ~ 5 microns were observed for the WAAM heat treated samples while the smallest sizes were observed for the EB-PBF and LP-DED fractured samples. Figure 4 illustrates these ductile dimple fracture features for the LP-DED AM process heat treated sample

series: using build power levels ranging from 350 W to 2620 W. In Figure 4 (a) the dimple size was ~ 2 microns (at 350 W) while the remaining fracture dimple sizes were ~3-4 microns. These features are consistent with corresponding grain width variations and the associated yield strength, e.g., 62 microns and 354 MPa at 350 W (Figure 4 (a) versus 114 microns and 336 MPa at 2620 W (Figure 4 (e)). These dimple sizes and corresponding grain sizes (widths), and yield stresses, are generally consistent with trends in a range of metal and alloy fractures where dimple size decreases with decreasing grain size and yield stress [16,17].

What is not necessarily consistent in these fracture ductile dimple size differences is the generally high elongation, which from Table 4 varies from a low of ~ 61 % to ~ 64 % for the LP-DED fracture surface series in Figure 4. In fact, the generally high elongations for all heat-treated components in Table 4 are somewhat unusual since the variation of yield stresses from 285 MPa for the WAAM heat treated components to 371 MPa for the L-PDF components show essentially the same elongation of ~ 56 %.



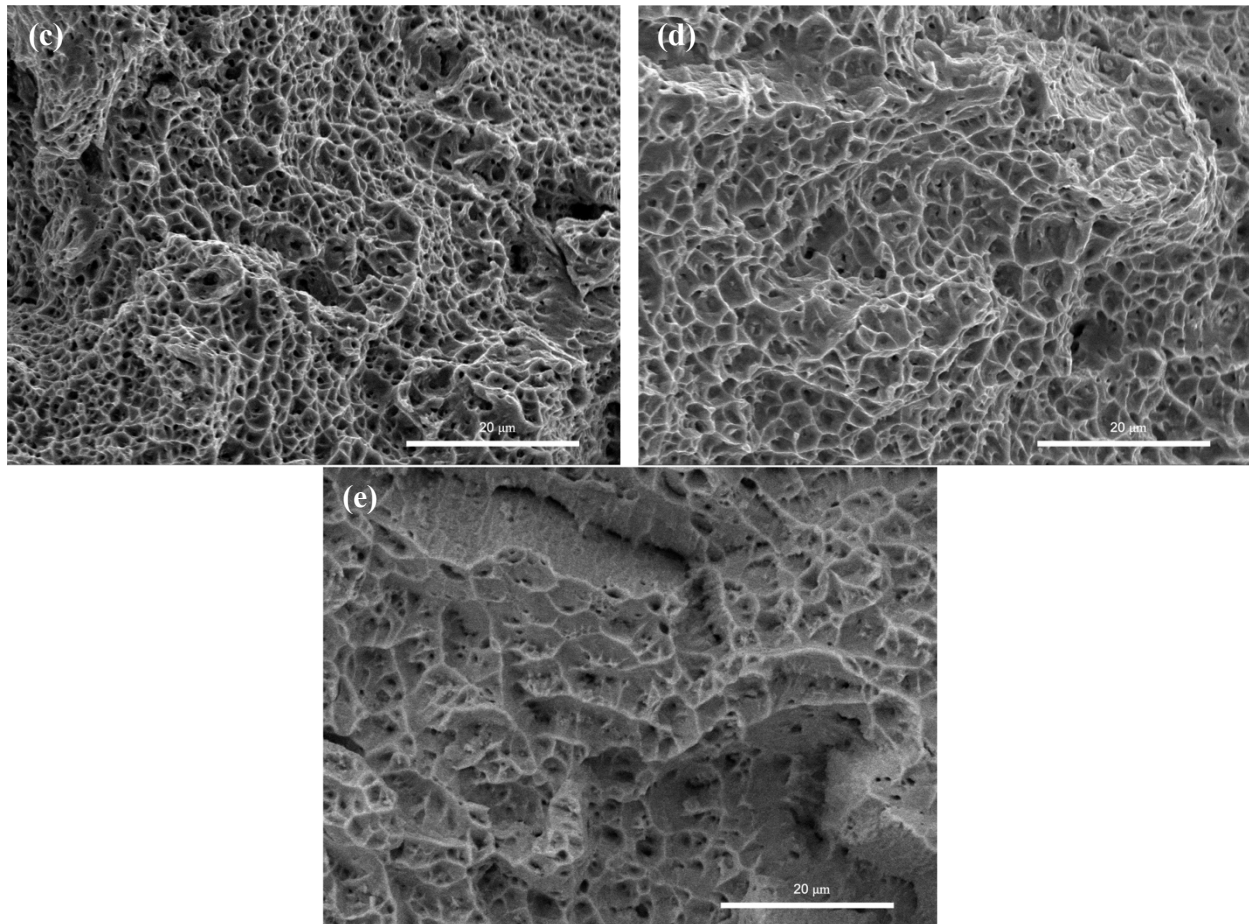


**Figure 4.** LP-DED heat treated SEM fractography images. (a) 350W, (b) 750W, (c) 1070W, (d) 2000W, (e) 2620 W.

### **Summary and Conclusions**

The reader can glean a graphic and comprehensive summary and overview of the results of this study by systematically reviewing (in sequence) Tables 3 and 4, and Figures 5 to 7. It is shown that various AM processes (Figure 2) can provide a range of residual, as-built properties which can be selectively enhanced or manipulated by high temperature heat treatment (SR + HIP + SOL). This study has provided a wide, comparative overview for Inconel 625 alloy product development and application optimization especially focused on mechanical properties: hardness and tensile. While wrought and cast Inconel 625 products can have hardness values ranging from ~ HV 180 to HV 320 after lower temperature aging (< 700 °C); corresponding to yield stress values ranging from 290 MPa (with elongations of ~ 65 %) to ~ 900 MPa (with elongations of ~ 31 %), AM processing and post-process heat treatments of Inconel 625 can produce a similar range of mechanical properties; with various AM processes providing a window of selections for optimizing specific applications. This study employed a range of 6 AM processes and compared properties of as-built components and high temperature heat treatments of these components. The as-built components showed a micro indentation hardness range of ~ HV 191 to HV 304; while the heat-treated component hardnesses ranged from HV

186 to HV 220. Yield stresses for the heat-treated components ranged from 285 MPa with 56 % elongation to 371 MPa with the same elongation.

In general, the important conclusions of this study include the following:

- \* A wide variety of AM process-built Inconel 625 products can be heat treated at high temperatures to produce desirable and optimal mechanical properties for specialized application optimization.
- \* AM processes such as WAAM, which invest large amounts of energy (heat) into the build have limited and low values of residual mechanical properties, including hardness, which is not significantly improved or altered with high temperature heat treatment.
- \* For LP-DED as-built products having process power ranging from 350 W to 2620 W, Vickers micro indentation hardness varied from HV 263 to HV 223, respectively while the heat-treated component hardness varied from HV 191 to HV 187, respectively; a variance of only 2 %.

## References

1. Floreen, S; Fuchs, G.F.; Yang, W.J. Metallurgy of alloy 625, *Superalloys 718,625 and Various Derivatives*, E. A Loria, Ed., The Minerals, Metals and Materials Society, Warrendale, PA, **2007**, 13-37.
2. Shankar, V.; Rao, K.B.S.; Mannan, S.L., Microstructure and mechanical properties of Inconel 625 superalloy. *J. Nuclear Mater.* **2001**,228,222-232.
3. Shoemaker, L.E., Alloys 625 and 725: Trends in properties and applications, *Superalloys 718, 625 and Various Derivatives*, E. A. Loria, Ed., The Minerals, Metals and Materials Society, Warrendale, PA, **2005**, 409-418.
4. Amato, K.N.; Hernandez, J.; Murr, L.E.; Martinez, E.; Gaytan, S.M.; Shindo, P.W., Comparison of microstructures and properties for a nickel-base superalloy (625) fabricated by electron and laser beam melting. *J. Mater. Sci. Res.* **2012**, 1, 1-41.
5. Marchese, G.; Lorusso, M.; Parizia, S.; Bassini, E.; Lee, J-W.; Calignano, F.; Manfredi, D.; Temer, M.; Hong, H-U.; Ugues, D.; Lombardi, M.; Biamino, S. Influence of heat treatments on microstructure evolution and mechanical properties of Inconel 625 processed by laser powder bed fusion. *Mater. Sci. Engr. A* **2018**, 729, 64-75.
6. Li, C.; White, R.; Fang, X.Y.; Weaver, M.; Gu, Y.B. Microstructure evolution characteristics of Inconel 625 alloy from selective laser melting to heat treatment. *Mater. Sci. Engr.*
7. Blakey-Milner, B.; Gradl, P.; Snedden, G.; Brooks, M.; Pitot, J.; Lopez, E.; Leary, M.; Berto, F.; du Plessis, A., Metal additive manufacturing in aerospace: A review. *Mater. Design.* **2021** 209, 110008. <https://doi.org/10.1016/j.matdes.2021.110008>
8. Gamon, A.; Arrieta, E.; Gradl, P.R.; Katsarelis, C.; Murr, L.E.; Wicker, R.B.; Medina, F. Microstructure and hardness comparison of as-built inconel 625 alloy following various additive manufacturing processes. *Results Mater.* **2021**, 12, 100239. <https://doi.org/10.1016/j.rinma.2021.100239>
9. DebRoy, T.; Wei, H.L.; Zuback, J.S.; Mukherjee, T.; Elmer, J.W.; Milewski, J.O.; Beese, A.M.; Wilson-Heid, A.; De, A., Zhang, W., Additive manufacturing of metallic components – Process, structure and properties. *Prog. Mater. Sci.* **2018**, 92, 112–224. <https://doi.org/10.1016/j.pmatsci.2017.10.001>
10. Schneider, C.A.; Rasband, W.S.; Eliceiri, K.W. NIH Image to ImageJ: 25 years of image analysis. *Nature Methods* **2012** 9, 671–675. <https://doi.org/10.1038/nmeth.2089>
11. Murr, L. E. *Interfacial Phenomena in Metals and Alloys*, Addison-Wesley Publishing Co., Reading, Mass. **1975**.
12. Trillo, E. A.; and Murr, L. E.; Effects of carbon content, deformation, and interfacial energetics on carbide precipitation and corrosion sensitization in 304 stainless steel. *Acta Mater.* **1999**.47 (1), 235-245.
13. Segura, I.A.; Murr, L.E.; Terrazas, C.A.; Bermudez, D.; Mireles, J.; Injeti, V.S.V.; Li, K.; Yu, B.; Misra, R.D.K.; Wicker, R.B. Grain boundary and microstructure engineering of Inconel 690 cladding on stainless steel 316L using electron beam powder bed fusion additive manufacturing. *J. Mater. Sci. & Technol.* **2019** 35, 351-367.

14. West, E.A.; Was, G.S. Grain boundary engineered 316L and 690 in supercritical water. *J. Nuclear Mater.* **2009** 392, 264-271.
15. Marchese, G.; Parizia, S.; Rashidi, M.; Saboori, A.; Manfredi, D.; Uges, D.; Lombardi, M.; Hryha, E.; Biamino, S. The role of texturing and microstructure evolution on the tensile behavior of heat-treated Inconel 625 produced by laser powder bed fusion, *Mater. Sci. Engr. A* **2020** 769, 138500.
16. Das, A.; Trafder, S. Geometry of dimples and its correlation with mechanical properties of stainless steel. *Scripta Mater.* **2008** 59(9), 1014-1017.
17. Qin, W.; Li, J.; Kang, J.; Zhu, L.; Shu, D.; et al. Effects of grain size on tensile property and fracture morphology of 316L stainless steel. *Mater. Lett.* **2019** 254, 116-119.

## List of Tables

**Table 1.** As-built AM process parameters.

**Table 2.** AM as-built sample identification and geometries.

**Table 3.** Summary of AM process microstructures and related properties for as-built components.

**Table 4.** Summary of AM process microstructures, mechanical and related properties for heat treated (SR + HIP + SOL) components.

## List of Figure Captions

**Figure 1.** Effect of temperature on metal alloy heat treatment (After ref. 10).

**Figure 2.** AM process schematic visualizations for layer building techniques used in this research.

**Figure 3.** LW-DED raster tool path.

**Figure 4.** L-PBF optical microscope images. (a) as-built, (b) heat treated.

**Figure 5.** WAAM optical microscope images. (a) as-built, (b) heat treated.

**Figure 6.** EB-DED optical microscope images. (a) as-built, (b) heat treated.

**Figure 7.** LP-DED optical microscope images. (a) 350 W as-built, (b) 350 W heat treated; (c) 750 W as-built, (d) 750 W heat treated; (e) 1070 W as-built, (f) 1070 W heat treated.

2620 W treated; (g) 2000 W as-built, (h) 2000W heat treated; (i) 2620 W as-built, (j) 2620 W heat treated.

**Figure 8.** EB-PBF optical microscope images. (a) as-built, (b) heat treated.

**Figure 9.** LW-DED optical microscope images. (a) as-built, (b) heat treated raster, (c) heat Treated raster 90, (d) heat treated linear 1.

**Figure 10.** LW-DED raster heat treated optical microscope image Higher magnification showing precipitates (dark spots).

**Figure 11.** Direct comparison of AW process grain widths for as-built and heat treated components.

**Figure 12.** Comparison of microhardness in the as-built and heat-treated condition for AM processes.

**Figure 13.** Summary of ultimate tensile strength and yield strength for heat treated AM process components.

**Figure 14.** LP-DED heat treated SEM fractography images. (a) 350 W, (b) 750 W, (c) 1070 W, (d) 2000 W, (e) 2620 W.